Chemical Bonds without “Chemical Bonding”? A Combined Experimental and Theoretical Charge Density Study on an Iron Trimethylenemethane Complex

Louis J. Farrugia,* Cameron Evans, and Marcus Tegel

WestCHEM, Department of Chemistry, University of Glasgow, Glasgow G12 8QQ Scotland

Received: March 24, 2006; In Final Form: May 8, 2006

High-resolution X-ray diffraction data, in conjunction with DFT(B3LYP) quantum calculations, have been used in a QTAIM analysis of the charge density in the trimethylenemethane (TMM) complex Fe(η^4-C{CH_2}$_3$)-$(CO)_3$. The agreement between the theoretical and experimental topological properties is excellent. Only one bond path is observed between the TMM ligand and the Fe atom, from the central C_α atom. However, much evidence, including from the delocalization indices and the source function, suggests that there is a strong chemical interaction between the Fe and C_β atoms, despite the formal lack of chemical bonding according to QTAIM.

1. Introduction

The quantum theory of atoms in molecules (QTAIM) of Bader[1] has enjoyed great popularity as a tool for charge density analysis.[2] Within the QTAIM, the idea of a *chemical bond* has no definable or identifiable physical form, and Bader[3] has suggested that this concept should be replaced with one of *chemical bonding* between nuclei. It is proposed[3] that a universal indicator of such chemical bonding is a shared interatomic surface and associated bond critical point (bcp) and bond path. A bond path is a unique trajectory in ρ between two atoms, where the density is maximal compared with any normal displacement, and where at the bcp (i.e., where $\nabla(\rho)$ is zero), it is minimal along that line. The topological properties of the density $\rho(\mathbf{r}_b)$ and the Laplacian of the density $\nabla^2\rho(\mathbf{r}_b)$ at the bcp may be used to classify[4] chemical interactions between atoms as either shared-shell (covalent) or closed-shell (ionic, van der Waals, H-bonded). This inductive approach works well for many examples of compounds of the light elements of periods 1 and 2. For heavier elements, such as the transition metals, where the bcp’s are invariably found in a region of charge depletion, the sign of $\nabla^2\rho(\mathbf{r}_b)$ alone is no longer a useful indicator of the nature of the chemical interaction. It is found necessary to extend the dichotomous scheme[4] by considering other topological criteria.[2b,5]

In the vast majority of cases, a bond path is found where “chemical intuition” leads us to expect a chemical bond, and the recovery of chemical structure must be considered as one of the triumphs of the QTAIM.[1] However, the association of a bond path with a chemical bond is neither straightforward nor uncontroversial.[3,6−9] Chemically unusual bond paths are sometimes observed, for instance, between F^- ions in LiF [6] or between the He and tertiary C atoms in He@$C_{10}H_{16}$.[7] Cioslowski et al.[8] initially proposed that these type of bond paths are associated with repulsive steric interactions. Bader has disagreed with this view[3] and has recently reiterated his opinion that the presence of a bond path always “implies not only the absence of repulsive Feynman forces on the nuclei, but also the presence of attractive Ehrenfest forces acting across the interatomic surface”.[9a]

The presence of extra, chemically unexpected bond paths is relatively common, and as pointed out by Coppens[2c] recently, QTAIM is being increasingly used to describe and understand unusual and/or weak intermolecular interactions. Indeed, the ubiquity of bond paths associated with weak intermolecular interactions has led some authors[10] to question their significance. However, the other case, i.e., the absence of a bond path where chemical intuition would lead us to expect a bond, is less well documented. One well-established example is a lack of a bond path for transition metal−metal interactions that are bridged by ligands such as CO[5a,11,12] or an alkylidyne.[13] Another example is the lack of basal B−B bond paths in the carbaborane $C_2B_3R_5$ as determined by both theory[14a,b] and experiment.[14c] In both these cases, it is worth noting that there are reasonable chemical arguments to support the lack of bonding. For instance, in $C_2B_3R_5$ one could argue that this compound does not have electron-deficient B−B bonds, despite the rather short B−B distances, but instead contains trigonal B atoms with electron precise bonds.[15]

A different class of complexes that illustrate this phenomenon are those involving π-bonded unsaturated hydrocarbyl ligands, such as the ubiquitous cyclopentadienyl ligand, which have a delocalized interaction between the metal center and the ligand. When the M(η^5-C_5H_5) fragment has exact C_{5v} symmetry, e.g., in ferrocene, the expected five bond critical points and bond paths between the M atom and the five ring C atoms are observed.[16] Associated with this ring of five bcp’s is a ring of five (3, +1) ring critical points (rcp), which have a very similar density ρ to that of the bcp’s. Identical topologies were observed for the M(η^5-C_5H_5) interactions in M(η^5-C_5H_5)$_2$ (M = Mg, Ca)[17a] and (η^5-C_5H_5)Mn$(CO)_2$(H)($SiCl_3$),[17b] but in other cases, particularly when the molecular symmetry is lower, then fewer bond paths between the formal η^5-C_5R_5 ligand and the metal may be found. For instance, in Ti(η^5-C_5H_5)(η^5-C_7H_9)[18a] only four Ti−Cp bp’s are observed, while for (MeC_5H_4)$(CO)_2$Mn-[η^2-O=C=C(μ-η^2-C≡CPh)$Co_2(CO)_6$Ph],[18b] only three Mn−MeCp bp’s are reported. Moreover, in Zr(2,4-C_7H_{11})[(*i*-Pr)-NCHPhCH$_2$CMe=CHCMe=CH$_2$], only one bond path is observed between the metal atom and both the (formally) η^4-butadiene and η^5-pentadienyl ligands.[19] The metal-ring topology in Na^+ π-complexes of substituted benzenes has also been

---

* Corresponding author. Fax +441413304888. E-mail address: louis@chem.gla.ac.uk.

10.1021/jp061846d CCC: $33.50

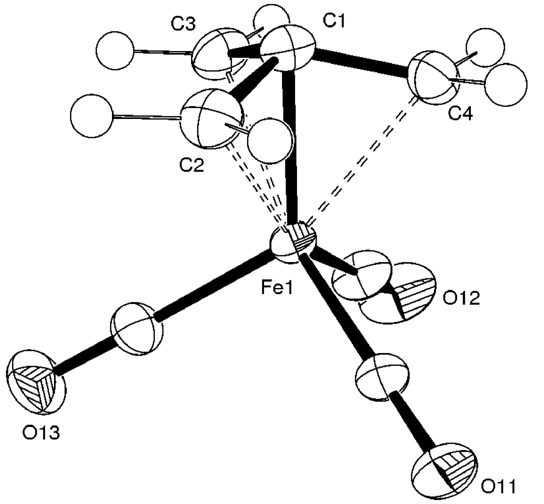

Figure 1. ORTEP diagram of **1**, showing the atomic labeling scheme. Ellipsoids are drawn at the 70% probability level, with H atoms represented as arbitrary spheres. Important metrical parameters: Fe(1)−C(1) = 1.9449(2), Fe(1)−C(2) = 2.1237(2), Fe(1)−C(3) = 2.1326(3), Fe(1)−C(4) = 2.1343(3), av Fe−C(O) = 1.7983(3), C(1)−C(2) = 1.4294(3), C(1)−C(3) = 1.4288(3), C(1)−C(4) = 1.4304(3) Å; Fe(1)−C(1)−C(2) = 76.310(14), Fe(1)−C(1)−C(3) = 76.729(14), Fe(1)−C(1)−C(4) = 76.769(14)°.

TABLE 1: Experimental Details[a]

compound formula	$C_7H_6FeO_3$
compound color	pale yellow
M_r	193.97
space group	$P2_1/c$
crystal system	monoclinic
a/Å	11.1211(2)
b/Å	6.86700(10)
c/Å	11.1440(2)
β/deg	113.7090(10)
V/Å^{-3}	779.22(2)
Z	4
D_{calc}/g cm^{-3}	1.653
$F(000)$	392
λ/Å	0.71073
μ(Mo-Kα)/mm^{-1}	1.885
crystal size/mm^3	0.58 × 0.38 × 0.33
transmission coefficients (range)	0.442−0.772
θ range/deg	3.58−49.1
$\sin(\theta_{max})/\lambda$	1.067
no. of data used for merging	197502
no. of unique data	7825
R_{int}	0.0332
R_σ	0.0115
Spherical Atom Refinement	
no. of data in refinement	7825
no. of refined parameters	125
Final R [$I > 2\sigma(I)$] (all data)	0.0190 (0.0215)
$R_w{}^2$ [$I > 2\sigma(I)$] (all data)	0.0537 (0.0545)
goodness of fit S	1.053
largest features in residual density map/e Å^{-3}	0.638(max) −1.132(min) 0.058(rms)
max shift/esd in last cycle	0.001
Multipole Refinement	
no. of data in refinement	7066
no. of refined parameters	301
Final R [$I > 3\sigma(I)$] (all data)	0.0110 (0.0151)
R_w [$I > 3\sigma(I)$]	0.0117
goodness of fit S	1.7098
largest features in residual density map/e Å^{-3}	0.227(max) −0.118(min) 0.03(rms)
max shift/esd in last cycle	$<1.0 \times 10^{-5}$

[a] $R = \sum(|F_o| - |F_c|)/\sum(F_o)$; $R_w = \{\sum[w(F_o - F_c)^2]/\sum[w(F_o)^2]\}^{1/2}$; $R_w{}^2 = \{\sum[w(F_o{}^2 - F_c{}^2)^2] / \sum[w(F_o{}^2)^2]\}^{1/2}$; $R_\sigma = \sum[\sigma(F_o{}^2)]/\sum [F_o{}^2]$; $R_{int} = \sum[n/(n-1]^{1/2}|F_o{}^2 - F_o{}^2(\text{mean})|/\sum F_o{}^2$ (summation is carried out only where more than one symmetry equivalent are averaged).

shown[20] to be highly dependent on the substituents. Bader has suggested[16,17b] that the interaction of a metal atom with a ring is best viewed as involving an interaction with the delocalized density of the entire ring perimeter—a viewpoint which accounts for the well-known fluxional mobility of such systems. This suggestion has not been further developed, and on the face of it seems in contradiction to the assertion[3] of the bond path as a universal indicator of chemical bonding between atoms.

The trimethylenemethane (TMM) ligand[21] is another interesting example of a delocalized π-hydrocarbyl ligand, one where the unsaturated C−C bonds are arranged in a stellated fashion rather than a ring or chain. The high formal valency of the central carbon atom renders the ligand unstable. In the free state, the molecule is a highly reactive[22] triplet radical, but on complexation to transition metals, it gives stable diamagnetic, closed-shell 18-electron compounds.[21] The compound Fe(η^4-C$\{CH_2\}_3$)(CO)$_3$ (**1**)[23] (Figure 1) was the first example of a TMM complex and is now used as a stereoselective reagent in organic synthesis.[24] It has been previously structurally characterized by X-ray diffraction in a thiourea cocrystal[25] and in the gas phase by electron diffraction,[26] but this article reports the first crystal structure of pure **1**. Our experimental and theoretical charge-density study on **1** provides a particularly clear-cut example of the absence of "expected" bond paths and highlights the difficulties in defining the nature of the interaction of a metal atom with a delocalized π-hydrocarbyl ligand within the AIM methodology.

2. Experimental Section

2.1. Synthesis. Compound **1** was prepared by the method of Ehrlich and Emerson.[23b] A mixture of $Fe_2(CO)_9$ (8.26 g, 22.71 mmol) and 2-chloromethyl-3-chloropropene (1.33 g, 10.0 mmol) in 60 mL diethyl ether was stirred at ambient temperature under a nitrogen atmosphere for 54 h. The resultant green−yellow solution was filtered, and most of the solvent and $Fe(CO)_5$ was carefully removed under reduced pressure. Kugelrohr distillation gave a crude yellow oil (0.9 mL) containing **1** and traces of $Fe(CO)_5$. Eight crystallization cycles from n-hexane at −96 °C afforded pure **1**. Complex **1** is a very volatile compound that melts close to ambient temperature (~27 °C). All attempts to grow a single crystal in a capillary directly from a melt by freeze−thaw cycles gave a plastic phase, with only a few, very intense, low-angle reflections. Further cooling below the freezing point gave a microcrystalline phase. Very large single crystals suitable for X-ray diffraction were finally grown by cooling liquid **1** containing a small amount of hexane at −5 °C over a period of several weeks in a refrigerator. These were moderately air stable and were handled on a glass plate cooled with solid CO_2 to prevent melting.

2.2. Data Collection, Processing, and Spherical Atom Refinement. Details of data collection procedures are given in Table 1. A single crystal of suitable size was cleaved from a much larger specimen. It was attached to a glass fiber using silicone grease and transferred rapidly to a goniometer head that was precooled at 100 K with an Oxford Instruments Series 7 Cryostream. Data were collected on a Nonius KappaCCD diffractometer, running under Nonius *Collect* software.[27a] The *Collect* software calculates and optimizes the goniometer and detector angular positions during data acquisition. A total of three runs were measured, using either ω- or φ-oscillation scans. In total, 3827 frame-images in 74 scan-sets were measured over a time period of 59.5 h. Run 2 used the same scan angles as run 1, but with a shorter exposure time to measure high-intensity low-angle data more accurately. The unit cell dimensions and errors were determined by postrefinement of the setting angles of the reflections from run 3, using the Scalepack program.[27b] The cell errors obtained from this least-squares procedure are undoubtedly serious underestimates[28] but are used here in the absence of better estimates. The frame images were integrated using *Denzo* (SMN),[27b] with a sufficiently large integration spot size to encompass the $K_{\alpha1-\alpha2}$ splitting, which becomes quite significant at $\theta \approx 50°$. In our experience, the neighborhood profiling used in *Denzo* (SMN) appears to cope quite well with the $K_{\alpha1-\alpha2}$ splitting, and a scatter plot of the individual scale factors after multipole refinement showed no significant trends (see Supplementary Information Figure S1). The resultant raw intensity files from *Denzo* (SMN) were processed using a locally modified version of *DENZOX*,[29] which calculates direction cosines for the absorption correction, as well as applying rejection criteria on the basis of bad χ^2 of profile-fit and ignoring partial reflections at the starting or final frame of a scan set. Absorption corrections by Gaussian quadrature,[30] based on the (approximated) crystal faces, were then applied to the reflection data. A second semiempirical correction[31] (without a θ-dependent correction) was applied to remove any residual absorption anisotropy due to the mounting medium and to account for other instrumental instabilities. Typical correction factors for the latter were in the range 1.0−0.85. A total of 197 502 intensity measurements were then sorted and merged using SORTAV,[32] giving 7825 independent data with a mean redundancy of 15.6. The dataset is 99.4% complete for $0 < \theta \leq 49.1°$, with only one missing low-angle reflection (1 0 0). A spherical atom refinement using *SHELXL97-2*[33] was initially undertaken, with full-matrix least-squares on F^2 and using all the unique data with the weighting scheme $w = [\sigma(F_o)^2 + (AP)^2 + BP]^{-1}$ where $P = [F_o{}^2/3 + 2F_c{}^2/3]$ and $A = 0.0279$, $B = 0.0977$. All non-H atoms were allowed anisotropic thermal motion. The hydrogen atom positions were obtained from a difference map and refined without restraints. The mean refined C−H distance was 0.95(2) Å. Neutral atom scattering factors, coefficients of anomalous dispersion, and absorption coefficients were obtained from ref 34. Details of this refinement are given in Table 1. Thermal ellipsoid plots were obtained using the program *ORTEP-3* for Windows.[35] All calculations were carried out using the *WinGX* package[36] of crystallographic programs.

2.3. Multipole Refinement. The multipole formalism of Hansen and Coppens[37] as implemented in the *XD* program suite[38] was used. The function minimized in the least-squares procedure was $\sum w(|F_o| - k|F_c|)^2$, with only those reflections with $I > 3\sigma(I)$ included in the refinement. The multipole expansion was truncated at the hexadecapole level for the Fe atoms, at the octapole level for the C and O atoms, and at the dipole level for the H atoms. The C−H distances were renormalized to 1.081 Å, this being the distance determined from a DFT geometry optimization (see below). In the absence of neutron diffraction data, the isotropic thermal parameters were estimated from a spherical atom refinement, using the contracted scattering factor of Stewart et al.[39] for the H atom. Each pseudoatom was assigned a core and spherical-valence scattering factor derived from the relativistic Dirac−Fock wave functions of Su and Coppens[40] expanded in terms of the single-ζ functions of Bunge, Barrientos, and Bunge.[41] The radial fit of these functions was optimized by refinement of the expansion−contraction parameter κ. The valence deformation functions for the O, C, and H atoms used a single-ζ Slater-type radial function multiplied by the density-normalized spherical harmonics. The radial terms used for the Fe atom were the relevant-order Fourier−Bessel transforms of the Su and Coppens[40] wave functions. The radial fits were optimized by refinement of their expansion−contraction parameters κ', with the same κ' parameter for all multipoles (KEEP KAPPA option in *XD*). Separate κ and κ' were used for the chemically distinct TMM and carbonyl C atoms. It is well-established[42] that the 3d transition metals pose special problems when refining the deformation density because of the significantly different radial extensions of the 3d and 4s valence orbitals. Attempts to refine the 4s population independently through the $l = 0$ deformation function (the second monopole) were unsuccessful; all such models proved unstable or gave physically unrealistic populations. In the model reported here, the 4s^2 scattering contribution is included as a fixed one in the "core" contribution. Adequate deconvolution of the thermal motion was judged by the Hirshfeld[43] rigid bond test, with a mean Δ-msda of 9.0×10^{-4} Å (max of 24×10^{-4} for Fe−C(3) Å).

The kinetic energy densities at the bcp's $G(\mathbf{r})$ given in Table 2 for the experimental densities were estimated using the approximation of Abramov[44]

$$G(\mathbf{r}) = ({}^{3}/_{10})(3\pi^2)^{2/3}\rho(\mathbf{r})^{5/3} + ({}^{1}/_{6})\nabla^2\rho(\mathbf{r})$$

while the corresponding potential energy densities at the bcp's $V(\mathbf{r})$ were obtained from the local virial

$$V(\mathbf{r}) = ({}^{1}/_{4})\nabla^2\rho(\mathbf{r}) - 2G(\mathbf{r})$$

This approximation[44] for $G(\mathbf{r})$ holds well in regions where $\nabla^2\rho(\mathbf{r}) > 0$ and is a good approximation for the Fe−C bonds in **1**. It is a much poorer approximation close to the nuclei or in regions of local charge concentration where $\nabla^2\rho(\mathbf{r})$ is negative and gives only qualitative results[45] in these cases, such as the C−C and C−H bonds.

2.4. Theoretical Studies. DFT(B3LYP) calculations were performed on **1** using the program *GAMESS-UK*,[46] with 6-311++G(2d2p) bases for the C, O, and H atoms and Wachters+f for Fe.[47] Properties were obtained from the wave function using the AIMPAC[48] suite of programs or AIM2000.[49] The properties reported herein were obtained from calculations at the optimized C_{3v} geometry (GEOM A), but essentially identical results were also obtained from calculations at the experimental geometry. Source functions[50] were calculated from the wave function using a modified version of PROAIMV kindly supplied by Carlo Gatti. Since the source function requires only knowledge of the density and its derivatives, it is, in principle, obtainable without approximation from the experimental density, though this option has not yet been coded. Calculations were also carried out at other geometries related to the normal modes of vibration of **1**. As detailed below, one such geometry, where the Fe−C$_\alpha$−C$_\beta$ angle is reduced from the equilibrium value to 72° (GEOM B), gives rise to bond critical points between the Fe and C$_\beta$ centers. The source function for the adduct H_3B−CO, calculated for comparison purposes as discussed below, was obtained from a DFT(B3LYP) wave function with optimized geometry, using 6-311++G(2d2p) bases for all atoms.

3. Results and Discussion

An ORTEP view is shown in Figure 1. The TMM ligand displays the usual "umbrella" conformation,[21] with the Fe atom being closer to the central C$_\alpha$ carbon than to the methylene C$_\beta$ carbons. In the previous X-ray structure determination of **1** as a cocrystal with thiourea,[25] molecules of **1** reside on a crystal-

TABLE 2: Topological Analysis of Bond Critical Points for (η^4-C_4H_6)Fe(CO)$_3$[a]

bond	R_b[b]	$d1$[b]	$d2$[b]	$\rho(\mathbf{r}_b)$[c]	$\nabla^2\rho(\mathbf{r}_b)$[d]	λ_1[d]	λ_2[d]	λ_3[d]	ϵ	$G(\mathbf{r}_b)$[e,f]	$G(\mathbf{r}_b)/\rho(\mathbf{r}_b)$	$V(\mathbf{r}_b)$[e]	$E(\mathbf{r}_b)$[e]
Fe−C(1)	1.9452	1.0245	0.9207	0.678(6)	8.470(8)	−1.53	−1.18	11.18	0.30	0.82	1.20	−1.04	−0.22
	1.9534	*1.0193*	*0.9341*	*0.665*	*7.987*	*−1.73*	*−1.73*	*11.44*	*0.00*	*0.75*	*1.13*	*−0.94*	*−0.19*
Fe−C(11)	1.7983	0.9159	0.8824	0.953(6)	13.105(14)	−4.33	−4.21	21.64	0.03	1.35	1.42	−1.79	−0.44
	1.8059	*0.8970*	*0.9089*	*0.927*	*13.999*	*−3.51*	*−3.40*	*20.91*	*0.03*	*1.30*	*1.41*	*−1.62*	*−0.32*
Fe−C(12)	1.7993	0.9141	0.8852	0.964(7)	13.287(14)	−4.43	−4.32	22.03	0.03	1.38	1.43	−1.82	−0.45
	1.8059	*0.8970*	*0.9089*	*0.927*	*13.999*	*−3.51*	*−3.40*	*20.91*	*0.03*	*1.30*	*1.41*	*−1.62*	*−0.32*
Fe−C(13)	1.7989	0.9052	0.8938	0.976(6)	13.704(15)	−4.52	−4.32	22.54	0.05	1.41	1.45	−1.86	−0.45
	1.8059	*0.8970*	*0.9089*	*0.927*	*13.999*	*−3.51*	*−3.40*	*20.91*	*0.03*	*1.30*	*1.41*	*−1.62*	*−0.32*
O(11)−C(11)	1.1463	0.3904	0.7559	3.247(16)	−2.22(13)	−34.58	−34.09	66.45	0.01	5.62	1.73	−11.4	−5.78
	1.1462	*0.3951*	*0.7511*	*3.128*	*7.499*	*−32.97*	*−32.94*	*73.40*	*0.00*	*5.94*	*1.90*	*−11.36*	*−5.42*
O(12)−C(12)	1.1469	0.3969	0.7500	3.296(16)	−13.54(13)	−34.63	−33.52	54.60	0.03	5.24	1.59	−11.42	−6.19
	1.1462	*0.3951*	*0.7511*	*3.128*	*7.499*	*−32.97*	*−32.94*	*73.40*	*0.00*	*5.94*	*1.90*	*−11.36*	*−5.42*
O(13)−C(13)	1.1496	0.3953	0.7543	3.260(17)	−9.01(14)	−34.06	−32.78	57.83	0.04	5.34	1.64	−11.32	−5.97
	1.1462	*0.3951*	*0.7511*	*3.128*	*7.499*	*−32.97*	*−32.94*	*73.40*	*0.00*	*5.94*	*1.90*	*−11.36*	*−5.42*
C(1)−C(2)	1.4298	0.7101	0.7197	1.939(11)	−14.731(26)	−14.11	−10.98	10.36	0.29	1.74	0.90	−4.50	−2.77
	1.4280	*0.7000*	*0.7280*	*1.940*	*−17.667*	*−14.05*	*−11.61*	*7.99*	*0.21*	*0.63*	*0.33*	*−2.50*	*−1.87*
C(1)−C(3)	1.4291	0.6948	0.7343	1.968(11)	−14.900(28)	−14.34	−11.01	10.45	0.30	1.79	0.91	−4.62	−2.83
	1.4280	*0.7000*	*0.7280*	*1.940*	*−17.667*	*−14.05*	*−11.61*	*7.99*	*0.21*	*0.63*	*0.33*	*−2.50*	*−1.87*
C(1)−C(4)	1.4307	0.7113	0.7193	1.922(10)	−14.421(26)	−13.79	−10.84	10.21	0.27	1.72	0.89	−4.44	−2.73
	1.4280	*0.7000*	*0.7280*	*1.940*	*−17.667*	*−14.05*	*−11.61*	*7.99*	*0.21*	*0.63*	*0.33*	*−2.50*	*−1.87*
C−H[g]	1.0812	0.7105	0.3707	1.837(33)	−16.80(42)	−17.08	−16.35	16.64	0.05	1.43	0.78	−4.04	−2.61
	1.0812	*0.6788*	*0.4024*	*1.937*	*−25.252*	*−18.54*	*−18.17*	*11.46*	*0.02*	*0.30*	*0.16*	*−2.37*	*−2.07*

[a] Top line experimental values, second line (italic) theoretical values from isolated molecule DFT calculation. [b] In units of Å. [c] In units of e Å^{-3}. [d] In units of e Å^{-5}. [e] In units of hartree Å^{-3}. [f] Estimated by the approximation of Abramov.[44] [g] Averaged values.

TABLE 3: Integrated Atomic Charges

atom	$q(\Omega)$[a]	$q(\Omega)$[b]	atom	$q(\Omega)$[a]	$q(\Omega)$[b]
Fe1	0.8098	0.8153	C12	0.9686	0.9885
O11	−1.1249	−1.1452	C13	0.9686	0.9159
O12	−1.1249	−1.0957	H21	−0.0026	0.0823
O13	−1.1249	−1.0367	H22	−0.0026	0.0977
C1	−0.0749	−0.0221	H31	−0.0026	−0.0137
C2	−0.0771	−0.2805	H32	−0.0026	0.0694
C3	−0.0771	−0.2711	H41	−0.0026	0.1033
C4	−0.0771	−0.2674	H42	−0.0026	0.0917
C11	0.9686	1.0052			
sum	0.019	0.0369			

[a] From DFT wave function. [b] From experimental density.

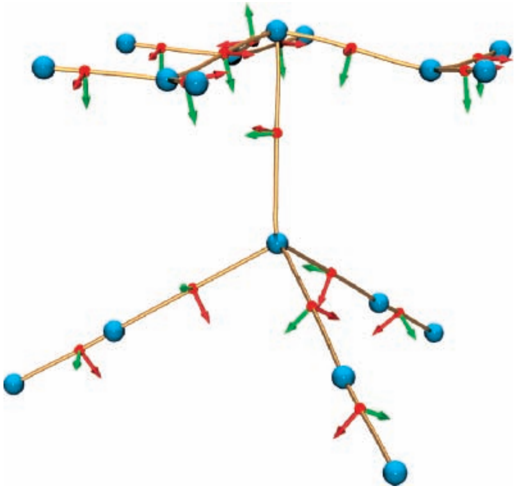

Figure 2. Experimental molecular graph of **1,** in the same view as Figure 1. Atomic centers are drawn as large blue spheres and bond critical points as small red spheres. The red and green arrows show, respectively, the directions of the minor and major principal axes of the ellipticity.

lographic threefold site, while in this structure, they lie in general positions, with no imposed symmetry. Nevertheless, the molecular geometry of **1** is close to the idealized C_{3v} symmetry and is essentially identical to the previous determinations.[25,26] However, the high accuracy of our determination shows there are small deviations from exact C_{3v} symmetry in the crystal phase—for instance, the Fe−C(2) distance differs from the other Fe−C$_\beta$ distances by substantially more than 3σ.

The deformation density maps (Figures S3−S5 and S8, Supporting Information) show the expected charge buildup in the covalent C−C and C−H bonds of the TMM ligand and in the Fe−C(O) and C−O bonds, but are quite ambiguous regarding the interaction between the TMM ligand and the Fe atom. There is no detectable redistribution of charge between Fe and C$_\alpha$ and only a suggestion of one between Fe and one of the C$_\beta$ carbon atoms C(4). More insight into the charge density in **1** is obtained through the QTAIM analysis of the charge density $\rho(\mathbf{r})$ reconstructed from the experimental atomic multipole populations. This gave the topological properties at the bcp's shown in Tables 2 and 3 and the molecular graph shown in Figure 2. The QTAIM analysis on the ab initio theoretical density at the DFT(B3LYP) level led to very similar results (Tables 2 and 3), and this excellent agreement gives us confidence in our description of the charge density in **1**. While we report here our calculations for the optimized C_{3v} geometry, our calculations on the experimental geometry gave essentially identical results. The atomic charges obtained by integration within the atomic basins (Table 3) indicate that the Fe atom, as expected, bears a small positive charge of ∼+0.81. This arises from an overall transfer of 0.12 e to each CO group and 0.41 e to the TMM ligand. The theoretically derived AIM charges indicate a slightly larger transfer of 0.15 e to each CO and a slightly smaller transfer of 0.32 e to the TMM ligand, but the overall charge on the metal is identical.

The topological properties at the bond critical points for the Fe−CO interactions (see Table 2) are similar to many previous experimental[11,13,51] and theoretical studies[5a,16] on transition metal−carbonyls and are now well-established as typical of their bond types.[2a,5a] These Fe−C bonds show moderate values for $\rho(\mathbf{r})$, positive values of the Laplacian $\nabla^2\rho(\mathbf{r})$, and negative values of the total energy density $E(\mathbf{r})$. As previously argued by Macchi and Sironi,[5a] these results are consistent with a considerable degree of covalency. The only notable disagreement between experiment and theory lies in the magnitudes of the Laplacian for the C−O bonds, which is a well-understood issue regarding

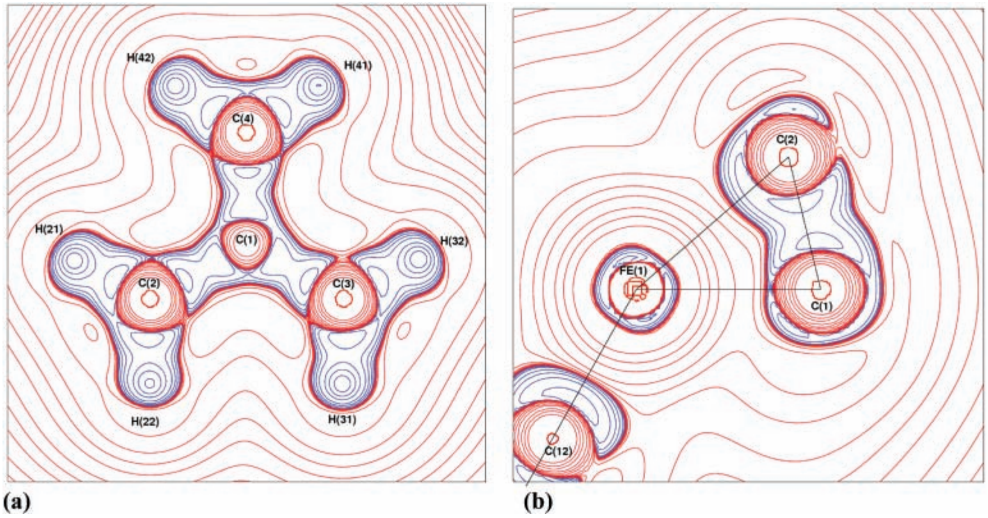

Figure 3. Plot of the experimental Laplacian $L \equiv -\nabla^2\rho(\mathbf{r})$ in the planes (a) C(2)−C(3)−C(4) and (b) Fe(1)−C(1)−C(2), with positive contours drawn in blue and negative contours in red. Contours are drawn at -1.0×10^{-3}, $\pm 2.0 \times 10^{n}$, $\pm 4 \times 10^{n}$, $\pm 8 \times 10^{n}$ ($n = -3, -2, -1, 0, +1, +2$) e Å^{-5}.

the position of the bcp.[5a,51] The topological properties at the Fe−C$_\alpha$ bcp imply a similar degree of covalency, but all the indicators suggest a weaker chemical bond than between Fe and the carbonyl C atoms.

The AIM analysis offers considerable insight into the bonding within the TMM ligand and its interaction with the Fe atom. The topological properties at the bcp's of the C−C bonds (Table 2) are clearly indicative of a substantial π-character. The high values of $\rho(\mathbf{r})$ and $\nabla^2\rho(\mathbf{r})$ resemble those for benzene,[52] and the major axes of the ellipticities ϵ lie normal to the plane containing the three C$_\beta$ (see Figure 2). The atomic graph of an atom, i.e., the set of critical points in $L(\mathbf{r}) \equiv -\nabla^2\rho(\mathbf{r})$ in the valence-shell charge concentration (VSCC) provides a graphic display of the distortions in the VSCC arising from chemical bonding.[1] The atomic graphs for Fe, C$_\alpha$, and C$_\beta$ have been obtained from both the theoretical and experimental densities and are evidently of the same topology (except that two critical points for the Fe graph could not be located in the experimental density). The atomic graphs of both C$_\alpha$ and C$_\beta$ (Figure S9, Supporting Information) show three (3, −3) cp's of charge concentration, which are approximately coplanar with the C atom and which lie along the directions of the covalent C−C or C−H bonds. This is good evidence for sp^2 hybridization for these atoms and is again consistent with their pseudo-benzenoid character. Both atoms C$_\alpha$ and C$_\beta$ have four (3, +1) cp's of charge depletion in their VSCC. For C$_\alpha$, one of these lies along the direction of the Fe− C$_\alpha$ axis and is aligned with a (3, −3) charge concentration in the VSCC of the Fe atom. This "lock and key" interaction[1,5a,16] is indicative of a donor−acceptor interaction between the Fe atom and the C$_\alpha$ of the TMM ligand (see Figure 3). The Fe atom has an atomic graph of the [8, 12, 6] cuboidal form (see Figure S9), which is quite typical[5a,13,51] of transition metals, having eight (3, −3) charge concentrations at the corners of a distorted cube, twelve (3, −1) saddle points, and six (3, +1) charge depletions in the face of the cube. Three of these (3, +1) charge depletions are oriented toward the three C$_\beta$ carbons, but there are no corresponding charge concentrations on these latter atoms. The other three (3, +1) charge depletions are associated in a "lock and key" fashion with the charge concentrations of the three CO ligands. The commonly accepted view that the L ligand in "piano-stool" complexes of the type LM(CO)$_3$ is associated with three of the metals' octahedral coordination sites is borne out by these observations.

The evidence regarding the nature of the Fe−C$_\beta$ interaction is ambiguous and is compounded by the molecular graph of **1** (Figure 2), which shows that *no bond critical point is observed* for any of the Fe−C$_\beta$ interactions. The topological interaction between the TMM ligand and the Fe center is thus described by a single bcp between Fe and C$_\alpha$. We stress that the lack of appearance of any Fe−C$_\beta$ bcp's in the experimental or optimized geometry is not a model-dependent feature—the same molecular graph is obtained regardless of the level of theory examined or of the elaboration of the multipole model used for the experimental study. This implies that, within Bader's definition,[3] there is no *chemical bonding* between the Fe and C$_\beta$ centers. This is a quite surprising result, especially in view of the observed "umbrella" conformation of the TMM ligand, which leads to shorter Fe−C$_\beta$ distances. The enhanced overlap[53] between the C$_\beta$ centers and the Fe(CO)$_3$ fragment resulting from this distortion is thought to be one of the main driving forces for the loss of planarity of the TMM ligand in metal complexes.

Moreover, there is much other physicochemical evidence that suggests that there is a significant Fe−C$_\beta$ π-interaction:

(a) A normal-mode analysis[54] of the vibrational spectrum of **1** shows that the ν(Fe−TMM) stretch has a large force constant of 3.7 mdyn/Å. The authors conclude that a model with a single bond from Fe to C$_\alpha$ is inadequate, and that significant π-interactions with the C−C bonds occur.

(b) ESCA[55] and photoelectron spectra[56] of **1** show that the donor/acceptor character of the TMM ligand resembles that of cyclobutadiene, i.e., strong π-interactions are indicated.

(c) The NMR barrier to rotation of the TMM ligand in complexes is generally found to be quite high,[21] again indicative of significant metal π-interactions. The electronic structure and rotational barrier of **1** has been investigated by Hoffmann et al.[53] These EHMO calculations show that rotation leads to a decrease in the interaction between the 2e and e″ orbitals, in turn leading to an increase in the energy of the HOMO. Moreover, the ^{13}C NMR chemical shifts of the C$_\beta$ carbons are much more sensitive to the peripheral ligands on the metal than the C$_\alpha$ carbon.[21]

(d) Our analysis of the Kohn−Sham orbitals from the DFT calculation shows the qualitative EHMO scheme of Hoffmann et al.[53] to be essentially correct. The frontier orbitals primarily responsible for the Fe−TMM bonding (15e and 18a$_1$, shown in Figure 4) imply significant Fe−C$_\beta$ interactions.

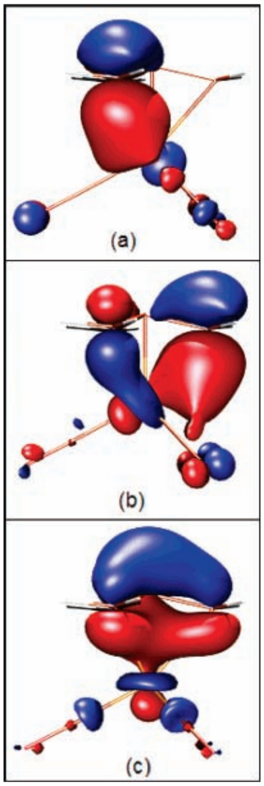

Figure 4. Frontier MOs of **1** which are primarily responsible for Fe−TMM bonding: the 15e orbitals in (a,b) and the $18a_1$ orbital in (c).

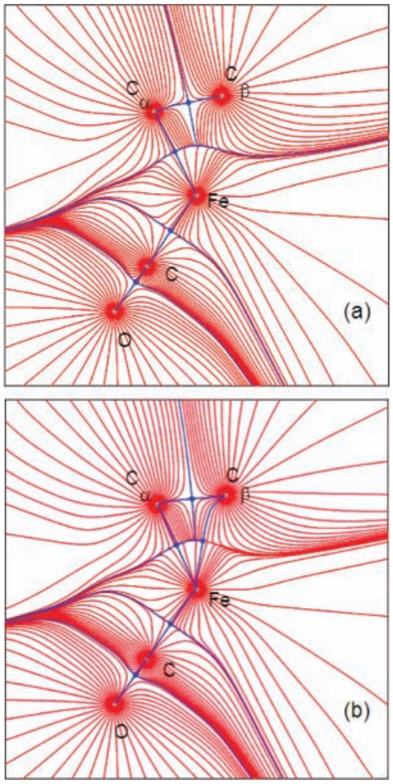

Figure 5. Plots of the gradient vector field of ρ for **1** in the plane $Fe-C_\alpha-C_\beta$: (a) for the optimized DFT geometry (GEOM A) and (b) for the TMM deformation geometry ($Fe-C_\alpha-C_\beta$ angle = 73°). Bond paths and zero-flux surfaces are shown in blue, with bcp's shown as blue solid circles.

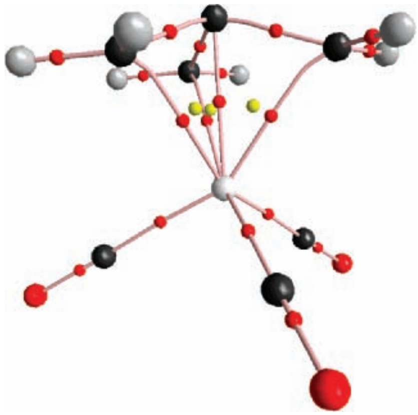

Figure 6. Molecular graph of **1** at GEOM B with $Fe-C_\alpha-C_\beta$ angle of 72°. Bond critical points are drawn as small red spheres and ring critical points as small yellow spheres.

TABLE 4: Delocalization Indices and Integrated Densities at Interatomic Surfaces

	$\delta(A, B)^a$	$\oint_{A\cap B}\rho(\mathbf{r})$, e Å$^{-1\ a}$	$\delta(A, B)^b$
$Fe-C_\alpha$	0.369	3.506	0.351
$Fe-C_\beta$	0.571		0.609
Fe−H	0.025		0.028
$Fe-C_{CO}$	1.045	2.162	1.026
C_α-C_β	1.204	3.534	1.191
C−H	0.966	1.882	0.959
C−O	1.605	3.170	1.600

[a] For equilibrium geometry A. [b] For nonequilibrium geometry B.

This evidence led us to consider more deeply the implications of the QTAIM analysis for **1**. The separatrix surfaces of $\nabla\rho(\mathbf{r})$, i.e., the zero-flux surfaces[57] separating the QTAIM atoms, are shown in the gradient vector field plot of **1** at the optimized geometry (Figure 5a). This figure graphically illustrates why there is no $Fe-C_\beta$ bond path. The trajectories of ρ within the basin of Fe follow the surface separating Fe from the C_α carbon. There are several normal modes[54] of vibration of **1** that lead to instantaneous reduction in the $Fe-C_\beta$ distance, and which might therefore generate a bcp for $Fe-C_\beta$. The average mean displacement amplitude of C_β in the direction of Fe is 0.12 Å, as determined from the thermal parameters at 100 K. Simulation of the molecular vibrations using DFT calculations on model geometries show that reducing the Fe−TMM separation along the $Fe-C_\alpha$ bond vector (corresponding to the symmetric ν(Fe−TMM) mode[54]) does not give rise to an $Fe-C_\beta$ bcp, even for unrealistically short $Fe-C_\alpha$ distances. On the other hand, the symmetric TMM deformation, where the $Fe-C_\alpha-C_\beta$ angle is reduced from the optimized equilibrium value of 76.6° to 73° (while retaining exact C_{3v} symmetry) results in a highly curved $Fe-C_\beta$ bond path (Figure 5b). At this geometry, the $Fe-C_\beta$ distance is 0.08 Å shorter, and the energy ~25 kJ mol^{-1} higher. The associated ring cp is extremely close to the new bcp, but a reduction in the $Fe-C_\alpha-C_\beta$ angle to 72° (geometry B, Figure 6) leads to a larger separation of these cp's and to a more (topologically) stable structure. Therefore, it seems likely that there are nonequilibrium geometries of **1**, instantaneously accessible through molecular vibrations, which do indeed possess an $Fe-C_\beta$ bond path and thus have a different molecular graph and hence AIM structure[1] from the equilibrium geometry.

It should be emphasized that, while the appearance of these bond paths is an "on or off" phenomenon, which may depend on very subtle features of the electron density, the overall features of the density in the two geometries are hardly different. Thus, the topological characteristics are almost unchanged from the equilibrium geometry (see Figure 5 and Table S4, Supporting Information). The new $Fe-C_\beta$ bcp and the associated rcp are only 0.24 Å apart, and their densities differ by only 0.007 e

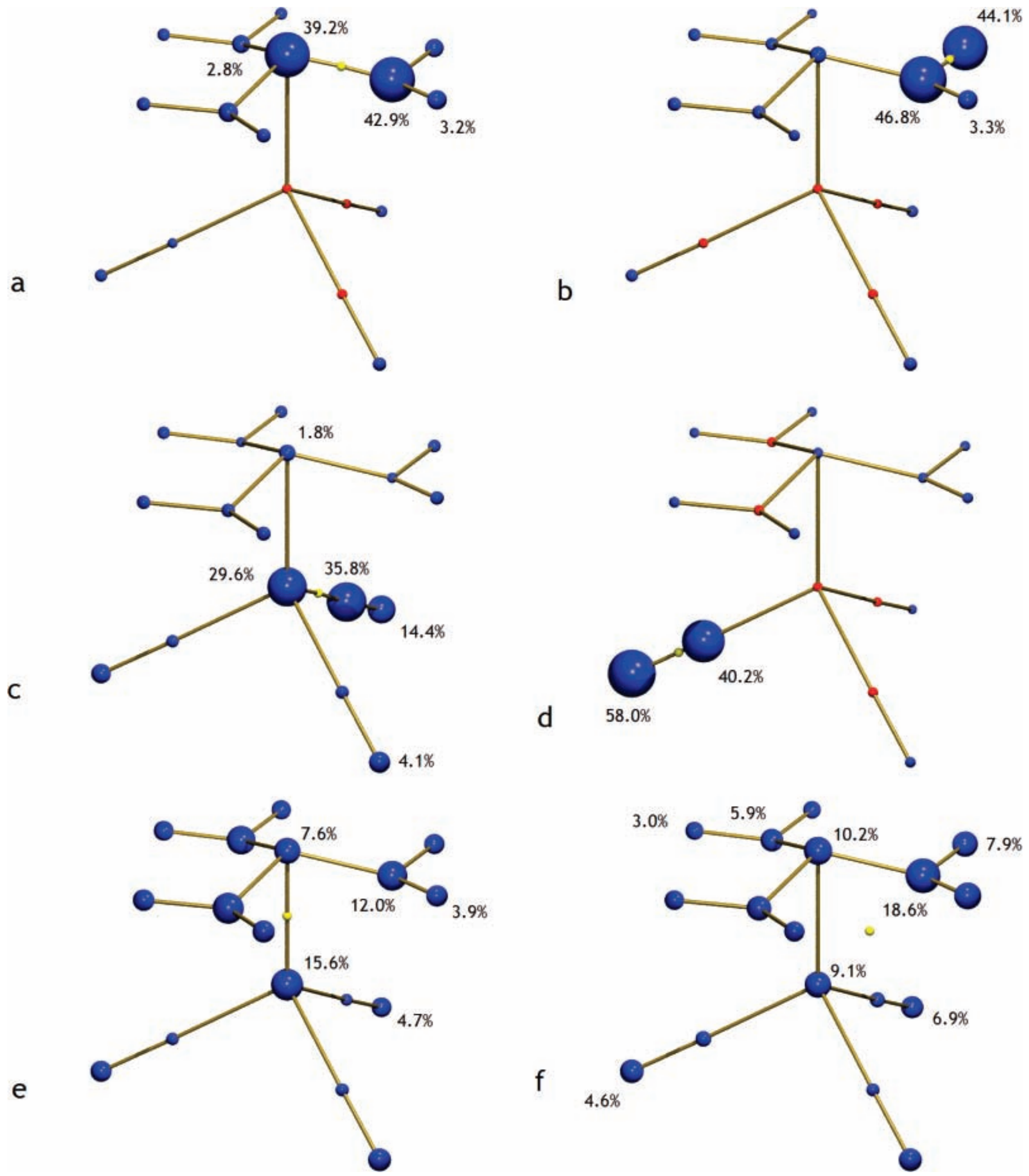

Figure 7. Percentage atomic source contributions to the electron density from the atomic basins of **1**, at the reference points (a) $C_\alpha-C_\beta$ bcp, (b) C−H bcp, (c) Fe−C(O) bcp, (d) C−O bcp, (e) $Fe-C_\alpha$ bcp, and (f) the $Fe-C_\beta$ midpoint. The volume of the spheres are proportional to the source contributions from the respective atomic basins, with positive contributions (sources) in blue and negative contributions (sinks) in red.

$Å^{-3}$, and moreover, they are very close in density to the $Fe-C_\alpha$ bcp (~0.65 $eÅ^{-3}$). As stated in the Introduction, Bader[16,17b] has proposed that the interaction of a metal atom with a cyclopentadienyl ring may best be viewed as an interaction with the delocalized ring density, and a similar situation is applicable in **1**. An isosurface plot of the density at 0.6 e $Å^{-3}$ (see Figure S10, Supporting Information) shows there to be a stellated ridge of isodensity connecting the Fe atom and the four TMM carbon atoms in geometry B, which is absent in the equilibrium geometry A. Consistent with this, we find that the new $Fe-C_\beta$ bcp is characterized by a high ellipticity (Table S4), the major axis of which is oriented toward the associated rcp. Finally, while we refer rather loosely to the atomic interaction lines and their associated (3, −1) critical points in the distorted geometry B as bp's and bcp's, this is not strictly applicable. As stated clearly by Bader,[1a,3] atomic interaction lines and their associated (3, −1) critical points in molecules can only be treated as bond paths and bond critical points when no forces are acting on the molecule. This is clearly not the case for geometry B, which is a nonequilibrium geometry. Nevertheless, it is commonly used terminology in the literature to refer to these topological features as bp's and bcp's in both cases (see ref 5a for several examples).

One QTAIM indicator that does not rely on the presence of a bond path is the delocalization index $\delta(A, B)$.[58] This index provides a measure of the Fermi correlation shared between two centers (and hence the number of electrons delocalized between the centers). The delocalization indices[59] for **1** are given in Table 4 and show the surprising result that $\delta(\mathrm{Fe}, C_\beta)$ is substantially *larger* than $\delta(\mathrm{Fe}, C_\alpha)$, despite there being no $Fe-C_\beta$ bond path. The sum of all δ(Fe, C) between the Fe atom and the TMM carbon atoms is 2.08, which is similar to the value of $\sum \delta(\mathrm{Fe}, \mathrm{C}) = 2.25$ reported[16] for the $Fe-C_5H_5$ interaction in ferrocene (from which it is suggested[16] that ~4 electrons are shared between the Fe atom and the C_5H_5 ring). While Bader emphasizes that the delocalization index does not provide a measure of bond order,[58b] since these indices exist for every atom pair, the same index proposed by Ángyán et al.[58c] is treated as a bond index. Moreover, in the presence of delocalized bonding, such as is found in the $Cr_2(\mu\text{-H})$ unit in $[Cr_2(\mu\text{-H})(CO)_{10}]^{-}$ [61] and in complex **1**, it becomes more difficult to

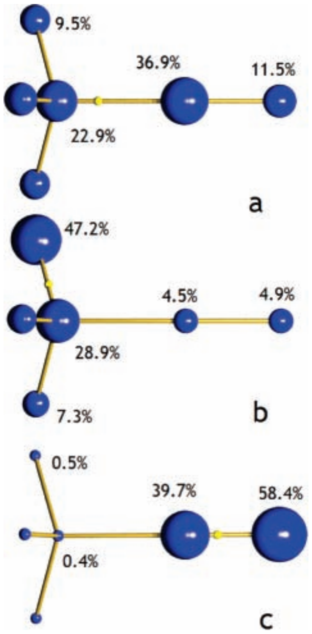

Figure 8. Percentage atomic source contributions to the electron density at (a) the B−C bcp, (b) the B−H bcp, and (c) the C−O bcp of H_3B-CO. The volume of the spheres is proportional to the source contributions from the respective atomic basins.

interpret the magnitude of $\delta(A, B)$. Nevertheless, it is quite unusual[62] to find the situation described here, where a formally *nonbonded* pair of atoms have a significantly larger $\delta(A, B)$ than a related *bonded* pair.

As originally suggested by Cremer and Kraka,[64] the integrated density over the zero flux surface shared by the two atoms, $\oint_{A\cap B}\rho(\mathbf{r}) = N(A, B)$, may provide a better measure of the strength of the interaction than just the density at the bcp, especially for interactions involving atoms with diffuse valence densities.[5a] The values of $N(A, B)$ for **1** at the equilibrium geometry A are given in Table 4. Unfortunately, those for geometry B with the Fe−C_β bond path are not available, since the surface integration fails in this case. The magnitudes of N(C−O), N(C−H), and $N(\mathrm{Fe-C_{CO}})$ are typical[5a] for interactions of their type. The magnitude of $N(\mathrm{Fe-C_\alpha})$ is considerably larger than that of $N(\mathrm{Fe-C_{CO}})$ and implies a strong interaction. Despite there being no bond path between Fe−C_β, and hence no shared interatomic surface, it is clear that there must be a considerable contribution of density toward $N(\mathrm{Fe-C_\alpha})$ from the C_β carbon atoms (see Figure 5).

Bader and Gatti[50a] have shown that it is possible to view the electron density at any point **r** within a molecule to consist of contributions from a source operating at all other points **r′**. The local source (LS) contribution at position vector **r** from **r′** is given by

$$-(^1/_4\pi)\int\frac{\nabla^2\rho(\mathbf{r}')}{|\mathbf{r}-\mathbf{r}'|}\,\mathrm{d}\mathbf{r}'$$

By integrating over the regions of space bounded by the zero-flux surfaces, the density may be equated to a sum of atomic contributions $S(\mathbf{r}, \Omega)$.

$$\rho(\mathbf{r}) = \sum_{\Omega}\int_{\Omega}\mathrm{LS}(\mathbf{r},\mathbf{r}')\,\mathrm{d}\mathbf{r}' \equiv \sum_{\Omega}S(\mathbf{r},\Omega)$$

The integrated form of the source function (SF) provides a measure of the relative importance of each atom's contribution to the density at a specific point. It has proved very useful in the characterization of hydrogen bonds[50b] according to the negative charge-, positive charge-, resonance-, and polarization-assisted H-bonding scheme of Gilli and Gilli[66] or as low-barrier H bonds.[50d] More recently, the SF has been used to define metal−metal interactions in bimetallic carbonyl complexes.[50e] The reference points **r** are normally taken at the bcp's—the least biased positions. Figure 7 shows the SF for **1** at the optimized geometry A, for a number of reference points **r**. Figure S11 (Supporting Information) shows the corresponding figure for geometry B. The source at the bcp's of the C_α−C_β, C−H, and C−O bonds (Figure 7a, b, and d) is substantially localized, with 82%, 91%, and 98% of the density, respectively, coming from the two atoms directly involved in the interaction. This is consistent with these bonds being treated as localized 2e-2c bonds. In contrast, the SF at the Fe−C(O) bcp (Figure 7c) has a significant additional contribution of 14% from the corresponding O atom. A similar situation has been observed previously[50e] for other metal carbonyl complexes, and it might be tempting to ascribe this to substantial Fe−CO π back-bonding. However, the SF for the donor−acceptor adduct H_3B-CO, shown in Figure 8, suggests that this is not the case. In this adduct, it is generally assumed[66] that any contribution from hyperconjugative π back-bonding is small;[67] the experimental value[68] for ν(CO) is $\sim$2167 cm^{-1}, above that for free CO and consistent with purely σ-donor interaction from the 5σ orbital of CO. The ratio of the contributions from the B, C, and O atoms at the B−C bcp is very similar to those for the Fe, C, and O contributions in **1**. This similarity is evidently not due to hyperconjugative π back-bonding, but may merely reflect a similarity in the delocalization in these bonds.

The most striking feature in the SF is seen when examining reference points for the Fe−TMM interaction. Here, the SF is strongly delocalized and does not differ greatly whether the reference point is taken as the Fe−C_α bcp or the Fe−C_β midpoint. Moreover, by comparing Figure 7 with Figure S11 (Supporting Information), it is clear that the SF contributions do not depend strongly on whether an Fe−C_β bcp is found or not. In all cases, the contribution from the C_β carbons atoms to the density at the reference point is greater than from the C_α carbon atom. It is interesting to note that the SF at these points show a small but significant contribution from the O atoms, but a much smaller contribution from the carbonyl C atoms. This delocalized distribution is also evident in the frontier MOs shown in Figure 4.

In conclusion, we have shown that, despite the fact that there is no bond path generated for the Fe−C_β interaction in **1** *at the equilibrium geometry*, there are a number of reasons (including two QTAIM indicators) for believing in a significant sharing of electrons between these centers. Moreover, a small distortion of the molecule, along the coordinate of a normal mode vibration, leads to the appearance of an Fe−C_β bond path. It is supposed that this combined evidence would lead most chemists to conclude that there is a *chemical bond* between these atoms, despite there being no *chemical bonding* in the sense of Bader.[3] We take the view, already expressed by Bader,[16,17b] that it is not profitable to view the interaction of transition metals with delocalized π-hydrocarbyl ligands solely in terms of localized M−C bond paths. Other tools, such as the delocalization indices[58] and the source function,[50] play a vital role in the AIM characterization of these chemical bonds.

Acknowledgment. We thank the EPSRC for grant GR/M91433 toward the purchase of a KappaCCD diffractometer. The New Zealand Foundation for Research, Science & Technology is thanked for financial (PDRA) support for C.E. We especially thank Drs. Piero Macchi and Carlo Gatti (Milano) for helpful discussions.

Supporting Information Available: Final refined parameters, observed and calculated structure factors in CIF format for the spherical atom and multipole refinements; supplementary figures (eight) of final residual maps, experimental deformation maps, dynamic and static model deformation maps, Laplacian maps, atomic graphs, and source function plots for GEOM B. This material is available free of charge via the Internet at http://pubs.acs.org.

References and Notes

(1) (a) Bader, R. F. W. *Atoms in Molecules: A Quantum Theory*; Oxford University Press: Oxford, 1990. (b) Popelier, P. *Atoms in Molecules: An Introduction*; Prentice Hall: Harlow, 2000.

(2) (a) Koritsanszky, T. S.; Coppens, P. *Chem. Rev.* **2001**, *101*, 1583−1628. (b) Gatti, C. *Z. Kristallogr.* **2005**, *220*, 399−457. (c) Coppens, P. *Angew. Chem.* **2005**, *44*, 6810−6811.

(3) Bader, R. F. W. *J. Phys. Chem. A* **1998**, *102*, 7314−7323.

(4) Bader, R. F. W.; Essén, H. *J. Chem. Phys.* **1984**, *80*, 1943−1960.

(5) (a) Macchi, P.; Sironi, A. *Coord. Chem. Rev.* **2003**, *238*, 383−412 and refs therein. (b) Gervasio, G.; Bianchi, R.; Marabello, D. *Chem. Phys. Lett.* **2004**, *387*, 481−484.

(6) Abramov, Y. A. *J. Phys. Chem. A* **1997**, *101*, 5725−5728.

(7) Haaland, A.; Shorokhov, D. J.; Tverdova, N. J. *Chem.*—*Eur. J.* **2004**, *10*, 4416−4421.

(8) (a) Cioslowski, J.; Mixon, S. T.; Edwards, W. D. *J. Am. Chem. Soc.* **1991**, *113*, 1083−1085. (b) Cioslowski, J.; Mixon, S. T. *Can. J. Chem.* **1992**, *70*, 443−449. (c) Cioslowski, J.; Mixon, S. T. *J. Am. Chem. Soc.* **1995**, *114*, 4383−4387. (d) Cioslowski, J.; Edgington, L.; Stefanov, B. B. *J. Am. Chem. Soc.* **1995**, *117*, 10381−10384.

(9) (a) Bader, R. F. W.; Fang, D.-C. *J. Chem. Theory Comput.* **2005**, *1*, 403−414. (b) Matta, F.; Hernández-Trujillo, J.; Tang, T.-H.; Bader R. F. W. *Chem.*—*Eur. J.* **2003**, *9*, 1940−1951. (c) Poater, J.; Solà, M.; Bickelhaupt, F. M. *Chem.*—*Eur. J.* **2006**, *12*, 2889−2895. (d) Bader R. F. W. *Chem.*—*Eur. J.* **2006**, *12*, 2896−2901. (e) Poater, J.; Solà, M.; Bickelhaupt, F. M. *Chem.*—*Eur. J.* **2006**, *12*, 2902−2905.

(10) Dunitz, J. D.; Gavezzotti, A. *Angew. Chem.* **2005**, *44*, 1766−1787.

(11) (a) Macchi, P.; Proserpio, D. M.; Sironi, A. *J. Am. Chem. Soc.* **1998**, *120*, 13429−13435. (b) Macchi, P.; Garlaschelli, L.; Martinengo, S.; Sironi, A. *J. Am. Chem. Soc.* **1999**, *121*, 10428−10429. (c) Macchi, P.; Garlaschelli, L.; Sironi, A. *J. Am. Chem. Soc.* **2002**, *124*, 14173−14184.

(12) Farrugia, L. J. *Chem. Phys. Lett.* **2005**, *414*, 122−126.

(13) Farrugia, L. J.; Evans, C. *C. R. Chim.* **2005**, *8*, 1566−1583.

(14) (a) Bader, R. F. W.; Legare, D. A. *Can. J. Chem.* **1992**, *70*, 657−676. (b) Jemmis, E. D.; Subramanian, G.; Srivvastava, I. H.; Gadre, S. R. *J. Phys Chem.* **1994**, *98*, 6445−6451. (c) Antipin, M.; Boese, R.; Bläser, D.; Maulitz, A. *J. Am. Chem. Soc.* **1997**, *119*, 326−333.

(15) This argument could of course be extended to the larger boranes and carbaboranes, but in these cases, basal B−B bond paths are usually observed. Note that ref 14a,b disagrees as to the presence of basal B−B bonding in $C_2B_4H_6$ and ref 14b states that no C−B bonding is observed at all in 1,7-$C_2B_5H_7$, an unrealistic situation which receives no further comment!

(16) Cortés-Guzman, F.; Bader, R. F. W. *Coord. Chem. Rev.* **2005**, *249*, 633−662.

(17) (a) Bytheway, I.; Popelier, P. L. A.; Gillespie, R. J. *Can. J. Chem.* **1996**, *74*, 1059−1071. (b) Bader, R. F. W.; Matta, C. F. *Inorg. Chem.* **2001**, *40*, 5603−5611.

(18) (a) Bader, R. F. W.; Matta, C. F.; Cortés-Guzman, F. *Organometallics* **2004**, *23*, 6253−6263. (b) Ortin, Y.; Lugan, N.; Pillet, S.; Souhassou, M.; Lecomte, C.; Costuas, K.; Saillard, J.-Y. *Inorg. Chem.* **2005**, *44*, 9607−9609.

(19) Pillet, S.; Wu, G.; Kulsomphob, V.; Harvey, B. G.; Ernst, R, D.; Coppens, P. *J. Am. Chem. Soc.* **2003**, *125*, 1937−1949.

(20) Cubero, E.; Orozco, M.; Luque, F. J. *J. Phys. Chem. A* **1999**, *103*, 315−321.

(21) Jones, M. D.; Kemmitt, R. D. W. *Adv. Organomet. Chem.* **1987**, *27*, 279−309.

(22) Dowd, P. *Acc. Chem. Res.* **1972**, *5*, 242−248.

(23) (a) Emerson, G. F.; Ehrlich, K.; Giering, W. P.; Lauterbur, P. C. *J. Am. Chem. Soc.* **1966**, *88*, 3172−3173. (b) Ehrlich, K.; Emerson, G. F. *J. Am. Chem. Soc.* **1972**, *94*, 2464−2470.

(24) Cox, L. R.; Ley, S. V. *Chem. Soc. Rev.* **1998**, *27*, 301−314.

(25) Tam, W.; Eaton, D. F.; Calabrese, J. C.; Williams, I. D.; Wang, Y.; Anderson, A. G. *Chem. Mater.* **1989**, *1*, 128−140.

(26) Almenningen, A.; Haaland, A.; Wahl, K. *Acta Chem. Scand.* **1969**, *23*, 1145−1150.

(27) (a) *Collect* data collection software; Nonius B.V., Delft: The Netherlands, 1999. (b) Otwinowski, Z.; Minor, W. Processing of X-ray Diffraction Data Collected in Oscillation Mode. In *Methods in Enzymology*; Carter, C. W., Jr., Sweet, R. M., Eds.; Academic Press: New York, 1997; Vol. 276 (Macromolecular Crystallography, part A), pp 307−326.

(28) Herbstein, F. H. *Acta Crystallogr., Sect. B* **2000**, *56*, 547−557.

(29) Blessing, R. H. *DENZOX*, program for processing Denzo x files; HWI, SUNY, Buffalo, 1997. Modified for KappaCCD data by Farrugia, L. J. and Muir, K. W., University of Glasgow: Glasgow, 2001.

(30) Coppens, P.; Leiserowitz, L.; Rabinovich, D. *Acta Crystallogr.* **1965**, *18*, 1035−1038.

(31) Sheldrick, G. *SADABS*, A Bruker-Nonius program for area detector absorption and other corrections, v. 2.10; University of Göttingen, Germany, 2003.

(32) Blessing, R. H. *J. Appl. Crystallogr.* **1997**, *30*, 421−426.

(33) Sheldrick, G. SHELXL-97, a program for crystal structure refinement; University of Göttingen, Germany, 1997; release 97-2.

(34) Tables 4.2.4.2, 4.2.6.8, and 6.1.1.4 In *International Tables for Crystallography, Volume C Mathematical, Physical and Chemical Tables*, Wilson, A. J. C., Kluwer: Dordrecht, 1995; pp 193−199, 219−222, 500−502.

(35) Farrugia, L. J. *J. Appl. Crystallogr.* **1997**, *30*, 565.

(36) Farrugia, L. J. *J. Appl. Crystallogr.* **1999**, *32*, 837−838.

(37) Hansen, N. K.; Coppens, P. *Acta Crystallogr., Sect. A* **1978**, *34*, 909−921.

(38) Koritsanszky, T.; Howard, S. T.; Richter, T.; Macchi, P.; Volkov, A.; Gatti, C.; Mallinson, P. R.; Farrugia, L. J.; Su, Z.; Hansen, N. K. *XD*, a computer program package for multipole refinement and topological analysis of charge densities from diffraction data; 2003.

(39) (a) Stewart, R. F.; Davison, E. R.; Simpson, W. T. *J. Chem. Phys.* **1965**, *42*, 3175−3187. (b) Stewart, R. F.; Bentley, J.; Goodman, B. *J. Chem. Phys.* **1975**, *63*, 3786−3793.

(40) Su, Z.; Coppens, P. *Acta Crystallogr., Sect A* **1998**, *54*, 646.

(41) Bunge, C. F.; Barrientos, J. A.; Bunge, A. V. *At. Data Nucl. Data Tables* **1993**, *53*, 113.

(42) Coppens, P. *Coord. Chem. Rev.* **1985**, *65*, 285−307.

(43) Hirshfeld, F. L. *Acta Crystallogr., Sect. A* **1976**, *32*, 239−244.

(44) Abramov, Y. A. *Acta Crystallgr., Sect. A* **1997**, *53*, 264−272.

(45) Gálvez, O.; Gómez, P. C.; Pacios, L. F. *Chem. Phys. Lett.* **2001**, *337*, 263−268.

(46) Guest, M. F.; Bush, I. J.; van Dam, H. J. J.; Sherwood, P.; Thomas, J. M. H.; van Lenthe, J. H.; Havenith, R. W. A.; Kendrick, J. *Mol. Phys.* **2005**, *103*, 719−747.

(47) Basis sets were obtained from the Extensible Computational Chemistry Environment Basis Set Database, version 02/25/04, as developed and distributed by the Molecular Science Computing Facility, Environmental and Molecular Sciences Laboratory, which is part of the Pacific Northwest Laboratory, P.O. Box 999, Richland, WA 99352, U.S.A., and funded by the U.S. Department of Energy. The Pacific Northwest Laboratory is a multiprogram laboratory operated by Battelle Memorial Institute for the U.S. Department of Energy under contract DE-AC06-76RLO 1830. Contact David Feller or Karen Schuchardt for further information.

(48) Biegler-König, F. W.; Bader, R. F. W.; Tang, T.-H. *J. Comput. Chem.* **1982**, *3*, 317.

(49) Biegler-König, F. *J. Comput. Chem.* **2000**, *12*, 1040.

(50) (a) Bader, R. F. W.; Gatti, C. *Chem. Phys. Lett.* **1998**, *287*, 233−238. (b) Gatti, C.; Cargnoni, F.; Bertini, L. *J. Comput. Chem.* **2003**, *24*, 422−436. (c) Gatti, C.; Bertini, L. *Acta Crystallogr., Sect. A* **2004**, *60*, 438−449. (d) Overgaard, J.; Schiott, B.; Larsen, F. K.; Iversen, B. B. *Chem.*—*Eur. J.* **2001**, *7*, 3756−3767. (e) Gatti, C. *Acta Crystallogr., Sect. A* **2005**, *61*, C47.

(51) Farrugia, L. J.; Evans, C. *J. Phys. Chem. A.* **2005**, *109*, 8834−8848.

(52) Bader, R. F. W.; Tang, T.-H.; Tal, Y.; Biegler-König, F. W. *J. Am. Chem. Soc.* **1982**, *104*, 946−952.

(53) Albright, T. A.; Hofmann, P.; Hoffmann, R. *J. Am. Chem. Soc.* **1977**, *99*, 7546−7557.

(54) Finseth, D. H.; Sourisseau, C.; Miller F. A. *J. Phys. Chem.* **1976**, *80*, 1248−1261.

(55) Koepke, J. W.; Jolly, W. L.; Bancroft, G. M.; Malmquist, P. A.; Siegbahn, K. *Inorg. Chem.* **1977**, *16*, 2659−2661.

(56) Dewar, M. J. S.; Worley, S. *J. Chem. Phys.* **1969**, *51*, 1672−1673.

(57) Bader, R. F. W. *Theor. Chem. Acc.* **2001**, *105*, 276−283.

(58) (a) Bader, R. F. W.; Stephens, M. E. *J. Am. Chem. Soc.* **1975**, *97*, 7391−7399. (b) Fradera, X.; Austen, M. A.; Bader, R. F. W. *J. Phys. Chem. A* **1999**, *103*, 304−314. (c) Ángyán, J. G.; Loos, M.; Mayer, I. *J. Phys. Chem.* **1994**, *98*, 5244−5248.

(59) The delocalization indices were computed from the DFT wave function, and are hence acceptable approximations, which are known to be generally slightly larger[60] than those obtained from HF wave functions.

(60) (a) Poater, J.; Solà, M.; Duran, M.; Fradera, X. *Theor. Chem. Acc.* **2002**, *107*, 362−371. (b) Wang, Y.-G.; Werstiuk, N. H. *J. Comput. Chem.* **2003**, *24*, 379−385.

(61) Macchi, P.; Donghi, D.; Sironi, A. *J. Am. Chem. Soc.* **2005**, *127*, 16494−16504.

(62) Delocalization indices between atoms not linked by a bond path are generally small, usually well below 0.1,[63a] but in cases where 3c-4e bonds are present in ABC interactions, these may become quite significant.[61,63] Nevertheless, the magnitudes of the "indirect" δ(A, C) are invariably smaller than those for the "direct" δ(A, B) and δ(B, C).

(63) (a) Matta, C. F.; Hernández-Trujillo, J.; Bader, R. F. W. *J. Phys. Chem A* **2002**, *106*, 7369−7375. (b) Molina, J. M.; Dobado, J. A. *Theor. Chem. Acc.* **2001**, *105*, 328−337. (c) Bochicchio, R.; Ponec, R.; Torre, A.; Lain, L. *Theor. Chem. Acc.* **2001**, *105*, 292−298. (d) Wang, Y.-G.; Werstiuk, N. H. *J. Comput. Chem.* **2003**, *24*, 379−385.

(64) Cremer, D.; Kraka, E. *Croat. Chem. Acta* **1984**, *57*, 1259−1281.

(65) Gilli, G.; Gilli, P. *J. Mol. Struct.* **2000**, *552*, 1−15.

(66) Goldman, A. S.; Krogh-Jespersen, K. *J. Am. Chem. Soc.* **1996**, *118*, 12159−12166.

(67) It has been suggested that the extent of hyperconjugative π-back-donation in $H_3B{-}CO$ is nonnegligible. See (a) Ermler, W. C.; Glasser, F. D.; Kern, C. W. *J. Am. Chem. Soc.* **1976**, *98*, 3799−3807. (b) Beach, D. B.; Jolly, W. L. *Inorg. Chem.* **1985**, *24*, 567−570. (c) Bauschlicher, C. W.; Ricca, A. *Chem. Phys. Lett*. **1995**, *236*, 14−19. Nevertheless, the delocalization index δ(B, C) in $H_3B{-}CO$ is only 0.47, which is much smaller than the typical values of ∼1 found[5a,13,16] for δ(M, C) in metal carbonyls, and suggests that hyperconjugative π-back-donation is not significant.

(68) (a) Bethke, G. W.; Wilson, M. K. *J. Chem. Phys.* **1957**, *26*, 1118−1130. (b) Jones, L. H.; Taylor, R. C.; Paine, R. T. *J. Chem. Phys.* **1979**, *70*, 749−756.